Theory for Vibrationally Resolved Two-Photon Circular Dichroism Spectra. Application to (*R*)-(+)-3-Methylcyclopentanone†

Na Lin,‡,§ Fabrizio Santoro,*,|| Antonio Rizzo,*,|| Yi Luo,‡ Xian Zhao,§ and Vincenzo Barone||

Department of Theoretical Chemistry, School of Biotechnology, Royal Institute of Technology, SE-10691 Stockholm, Sweden, Institute of Crystal Materials, Shandong University, 250100 Jinan, Shandong, People's Republic of China, and Istituto per i Processi Chimico-Fisici del Consiglio Nazionale delle Ricerche (IPCF-CNR), Area della Ricerca, Via G. Moruzzi 1, I-56124 Pisa, Italy

Received: December 2, 2008; Revised Manuscript Received: January 15, 2009

A harmonic adiabatic approach in combination with density functional response theory for computing two-photon vibronically resolved circular dichroism spectra of chiral molecules is presented. It includes both Franck−Condon and Herzberg−Teller contributions and it takes fully into account frequency changes and Duschinsky effects. Model calculations have been performed for two dominant conformers of (*R*)-(+)-3-methylcyclopentanone in the gas phase. It is found that the Herzberg−Teller contribution can introduce a sign change in two-photon circular dichroism of a single excited electronic state of a conformer. The change survives after Boltzmann averaging, and it might be amenable to experimental verification. Interesting interference effects between Franck−Condon and Herzberg−Teller contributions are revealed and analyzed in detail. Results obtained within the more approximate and less computationally intensive linear coupling vibronic model are also given for comparison.

1. Introduction

Two-photon circular dichroism (TPCD)[1] arises from the difference in two-photon absorption of left and right circularly polarized light. It combines the advantages of two-photon absorption (TPA), that is 3D confocality, reduced frequency, enhanced penetration power, and so forth,[2] with the fingerprinting capabilities of electronic circular dichroism (ECD).[3−5] Great interest in TPCD has recently been revived thanks to the development of new theoretical approaches.[6−9] Experimental verification has proven to be rather challenging. On the basis of the theoretical work of Szłucki and Stręk,[10] focusing on the TPCD of specific electronic transitions in Lanthanide complexes, Gunde and Richardson measured the fluorescence-detected two-photon circular dichroism of uniaxial crystals of a Gadolinium complex.[11] Nonlinear circular dichroism induced by radiation was also studied theoretically[12] and observed in liquid samples of ruthenium bipyridil salts[13−16] a few years ago by Hache and co-workers. In 2004, Markowicz and co-workers introduced a modified Z-scan technique that helped establish upper limits for the two-photon dichroism that could be detected.[17] Very recently, Hernández and co-workers made a remarkable progress in the experimental measurement of TPCD by developing a double L-scan technique,[18] which can yield well resolved TPCD and two-photon linear-circular dichroism (TPLCD, defined essentially as the difference between circularly and linearly polarized TPA) spectra for chiral samples in solution. Progresses in both theoretical modeling and experiment could therefore make TPCD a promising tool for various applications in biology, pharmaceutical, medical, and nanoscience.

Theoretical studies of TPCD have been mainly focused on purely electronic contributions.[8,9,19] However, as shown in our recent studies on ECD of (*R*)-(+)-3-methylcyclopentanone (R3MCP),[20,21] vibronic effects could have a profound impact on the rotatory strengths of selected excitations. It was found that non-Condon vibronic effects such as those yielded by the Herzberg−Teller (HT) contribution could introduce a change of sign to the ECD response of the molecule. This fact has important consequences on the assignment of absolute configuration of chiral systems.[20,21] The importance of vibronic effects on ECD spectra was also highlighted by recent studies carried out by Neugebauer, Nooijen, and co-workers,[22,23] and by Dierksen and Grimme.[24]

In this article, we investigate how vibronic coupling modulates TPCD response. To this end, we present a detailed analysis of the vibronic structure of TPCD spectra based on accurate first-principle calculations, with a full account of Franck−Condon (FC) and HT contributions. Already a long time ago,[25] it was realized that for a reliable treatment of HT effects in one-photon absorption and emission spectra computed in harmonic approximation, Duschinsky mixing[26] of the normal coordinates of the electronic states involved in the electronic transition must be taken into account because it modulates the interferential patterns ultimately giving rise to vibronic transition intensities. It may be expected that such interferences are even more relevant in the determination of the intensities of complex signals as TPCD, which depend on the combined effects of the electric and magnetic dipole and the electric quadrupole transition moments (section 2.1). In ref 27, an effective method for the computation of vibronically resolved one-photon optical spectra of large molecules was developed in the harmonic approximation, including both Duschinsky rotation and the effect of finite temperature both in the gas phase and in solution. In this framework, FC spectra can be computed through the evaluation of the overlaps of multidimensional vibrational states. Generalizations have been made to introduce also HT effects.[28] In

† Part of the "George C. Schatz Festschrift".

* To whom correspondence should be addressed. E-mail: f.santoro@ipcf.cnr.it (F.S.), rizzo@ipcf.cnr.it (A.R.).

‡ Royal Institute of Technology.

§ Shandong University.

|| Istituto per i Processi Chimico-Fisici del Consiglio Nazionale delle Ricerche (IPCF-CNR).

10.1021/jp8105925 CCC: $40.75
Published on Web 03/02/2009

the literature, this method has been sometimes defined as the "harmonic adiabatic FC approach" (AFC) by Nooijen and co-workers.[29,30] The complex nature of the signal to be simulated for TPCD poses technical challenges because robust and effective methods are needed to obtain fully converged vibrationally resolved TPCD signals, which can result from sums of positive and negative contributions with possible issues due to partial or total cancelation effects. To face this problem, we generalized the method developed in refs 27, 28 for one-photon spectra to deal with two-photon processes, and here we present to the best of our knowledge the first − exact in harmonic approximation − simulation and analysis of vibrationally resolved TPCD. The combined effects of equilibrium structure displacements, frequency changes, and Duschinsky mixing in the radiative transition will be analyzed in detail. Furthermore, to highlight the HT modulation of the spectral lineshapes, TPCD spectra will be compared with one-photon absorption (OPA) and ECD spectra, and with TPA spectra. We choose the two dominant conformers of R3MCP as our model systems. R3MCP was indeed the subject of a combined linear and nonlinear circular dichroism experimental study,[31,32] and, also due to its well characterized excitation spectrum, it is in our view an ideal reference system for a comparison of the four linear and nonlinear spectroscopies mentioned above. The computation of harmonic AFC spectra requires the determination of the equilibrium structures of all of the excited electronic states lying within the energy window of interest, and this may become a cumbersome task for sizable molecules. For this reason, results with a simpler approach, the so-called linear coupling model (LCM),[33] are also given for comparison. LCM, also known as the gradient FC (GFC) approach, assumes that the normal modes and frequencies are the same in the initial and final electronic states, whereas the equilibrium geometries are displaced. The displacement can be estimated from the excited-state energy gradients computed at the ground-state equilibrium geometry. Although LCM is expected to perform best in the simulation of low-resolution spectra, it has been already successfully adopted to capture the major features of many one- and two-photon absorption processes.[34−36]

In section 2 the theoretical framework will be briefly sketched. Computational details follow in section 3. The results of our study are presented and discussed in section 4, whereas section 5 collects our main conclusions.

2. Theory

2.1. Basic Formalism for Vibronically Resolved TPCD and TPA. In refs 20 and 21, we have summarized the theory for vibronically resolved ECD. Here, we report the main expression for the observable and use it to introduce our formalism. The anisotropy of the molar absorptivity $\varepsilon(\omega)$, a function of the laser frequency ω, defined as the difference between the one-photon absoptivity for left (L) and right (R) circularly polarized light, $\Delta\varepsilon(\omega) = \varepsilon_L(\omega) - \varepsilon_R(\omega)$, can be written as[19]

$$\Delta\varepsilon^{\mathrm{ECD}}(\omega) = \frac{16\times(2\pi)^2\times\omega\times N_A}{9\times1000\times\ln(10)\times(4\pi\varepsilon_0)\times\hbar c_0^2}\times \sum_f\sum_{v_g,v_f} p_{v_g}\, g(\omega,\omega_{gv_gfv_f})\times {}^{gv_gfv_f}R \approx 2.73719\times10^{-2}\times\omega\times\sum_f\sum_{v_g,v_f} p_{v_g}\, g(\omega,\omega_{gv_gfv_f})\times {}^{gv_gfv_f}R \quad (1)$$

In eq 1, $\omega_{gv_gfv_f}$ is the transition energy from the initial state $|gv_g\rangle$ to the final state $|fv_f\rangle$, where v_g and v_f are the vibrational states of the electronic initial g and final f states, respectively. $g(\omega,\omega_{gv_gfv_f})$ is the normalized line shape function (either a Lorentzian or a Gaussian depending on which between homogeneous and inhomogeneous broadening is dominant), N_A is Avogadro's number, c_0 the speed of light in vacuo and ε_0 the vacuum permittivity. p_{v_g} is the Boltzmann population of $|v_g\rangle$. Our spectra assume transitions from the vibrational ground-state, which is dominant in the Boltzmann distribution. The ECD rotatory strength,[37,38] R, entering eq 1 is proportional to the imaginary part of the scalar product of the electric dipole ($\hat{\mu}$) and magnetic dipole ($\hat{m}$) transition moments,

$${}^{gv_gfv_f}R = \frac{3}{4}\sum_{\alpha=x,y,z}\Im\left[\mu_\alpha^{gv_gfv_f} m_\alpha^{gv_gfv_f*}\right] \quad (2)$$

where $\mu_\alpha^{gv_gfv_f} = \langle gv_g|\mu_\alpha|fv_f\rangle$ and $m_\alpha^{gv_gfv_f} = \langle gv_g|m_\alpha|fv_f\rangle$, μ_α is the α Cartesian component of $\hat{\mu}$

$$\mu_\alpha = \sum_i q_i r_{i\alpha} \quad (3)$$

and m_α is the α component of $\hat{m}$

$$m_\alpha = \sum_i \frac{q_i}{2m_i} l_{i\alpha} = \sum_i \frac{q_i}{2m_i}(r_i\times p_i)_\alpha \quad (4)$$

In eqs 3 and 4, the Cartesian components of the position ($r_{i\alpha}$), linear momentum ($p_{i\alpha}$), and angular momentum ($l_{i\alpha}$) of the particles of charge q_i and mass m_i appear. The expression of vibronic OPA is very similar to that of vibronic ECD, eq 1

$$\varepsilon^{\mathrm{OPA}}(\omega) = \frac{(2\pi)^2\times\omega\times N_A}{3\times1000\times\ln(10)\times\hbar c_0\times(4\pi\varepsilon_0)}\times \sum_f\sum_{v_g,v_f} p_{v_g}\, g(\omega,\omega_{gv_gfv_f})\sum_{\alpha=x,y,z}\left|\mu_\alpha^{gv_gfv_f}\right|^2 \approx 2.81320\times\omega\times\sum_f\sum_{v_g,v_f} p_{v_g}\, g(\omega,\omega_{gv_gfv_f})\sum_{\alpha=x,y,z}\left|\mu_\alpha^{gv_gfv_f}\right|^2 \quad (5)$$

The last rows of eqs 1 and 5 yield the ECD and OPA observables in units of $dm^3\ mol^{-1}\ cm^{-1}$ starting from circular frequencies and transition dipole moments given in atomic units.

In this article, we focus on the theory of vibronic two-photon processes. TPCD was theoretically described by Tinoco, Jr., in the 1970s[1] and also by Power,[39−41] and Andrews.[42] In ref 6, definitions were given and a computational approach to the ab initio determination of TPCD spectra was discussed. In ref 7, a selection of origin invariant approaches was presented. The one based on Tinoco's original formulation, labeled as the TI approach, is employed in our present study. For two photons of equal frequency ω, starting from the expressions given in refs 1 and 7, the TPCD, $\Delta\delta^{TPCD}(\omega) = \delta_L(\omega) - \delta_R(\omega)$, can be written as

$$\Delta\delta^{\mathrm{TPCD}}(\omega) = \frac{4}{15}\frac{(2\pi)^2\times\omega^2\times N_A}{c_0^3\times(4\pi\varepsilon_0)^2}\times \sum_f\sum_{v_g,v_f} p_{v_g}\, g(2\omega,\omega_{gv_gfv_f})\times {}^{gv_gfv_f}R_{\mathrm{TPCD}} \approx 4.67299\times10^{-32}\times\omega^2\times\sum_f\sum_{v_g,v_f} p_{v_g}\, g(2\omega,\omega_{gv_gfv_f})\times {}^{gv_gfv_f}R_{\mathrm{TPCD}} \quad (6)$$

The circular frequency is assumed throughout to be the same for the two absorbed photons. ${}^{gv_gfv_f}R_{\mathrm{TPCD}}$ in eq 6 is the TPCD rotatory strength, and it can be obtained in an origin invariant

form, independent of the completeness of the one-electron basis set employed in the calculation, as[7]

$$ {}^{g\nu_g f\nu_f}R_{\mathrm{TPCD}} = -b_1 B_1^{\mathrm{TI}}(\omega) - b_2 B_2^{\mathrm{TI}}(\omega) - b_3 B_3^{\mathrm{TI}}(\omega) \quad (7) $$

The results presented in this work correspond to an experimental setup with two left circularly polarized beams propagating parallel to each other. For this arrangement, $b_1 = 6$, and $b_2 = -b_3 = 2$.[1]

$$ B_1^{\mathrm{TI}}(\omega) = \frac{1}{\omega^3}\sum_{\rho\sigma} M_{\rho\sigma}^{p,g\nu_g f\nu_f}(\omega) P_{\rho\sigma}^{p,g\nu_g f\nu_f *}(\omega) \quad (8) $$

$$ B_2^{\mathrm{TI}}(\omega) = \frac{1}{2\omega^3}\sum_{\rho\sigma} T_{\rho\sigma}^{+,g\nu_g f\nu_f}(\omega) P_{\rho\sigma}^{p,g\nu_g f\nu_f *}(\omega) \quad (9) $$

$$ B_3^{\mathrm{TI}}(\omega) = \frac{1}{\omega^3}\sum_{\rho\sigma} M_{\rho\rho}^{p,g\nu_g f\nu_f}(\omega) P_{\sigma\sigma}^{p,g\nu_g f\nu_f *}(\omega) \quad (10) $$

Summations in eqs 8−10 run over Cartesian (x, y, z) components. The tensors $P_{\alpha\beta}^{p,g\nu_g f\nu_f}(\omega)$, $M_{\alpha\beta}^{p,g\nu_g f\nu_f}(\omega)$, and $T_{\alpha\beta}^{+,g\nu_g f\nu_f}(\omega)$ are defined by the sum-over-state expressions

$$ P_{\alpha\beta}^{p,g\nu_g f\nu_f}(\omega) = \frac{1}{\hbar}\sum_{k,\nu_k}\left[\frac{\langle g\nu_g|\mu_\alpha^p|k\nu_k\rangle\langle k\nu_k|\mu_\beta^p|f\nu_f\rangle}{\omega_{k\nu_k} - \omega} + \frac{\langle g\nu_g|\mu_\beta^p|k\nu_k\rangle\langle k\nu_k|\mu_\alpha^p|f\nu_f\rangle}{\omega_{k\nu_k} - \omega}\right] \quad (11) $$

$$ M_{\alpha\beta}^{p,g\nu_g f\nu_f}(\omega) = \frac{1}{\hbar}\sum_{k,\nu_k}\left[\frac{\langle g\nu_g|\mu_\alpha^p|k\nu_k\rangle\langle k\nu_k|m_\beta|f\nu_f\rangle}{\omega_{k\nu_k} - \omega} + \frac{\langle g\nu_g|m_\beta|k\nu_k\rangle\langle k\nu_k|\mu_\alpha^p|f\nu_f\rangle}{\omega_{k\nu_k} - \omega}\right] \quad (12) $$

$$ T_{\alpha\beta}^{+,g\nu_g f\nu_f}(\omega) = \frac{1}{\hbar}\varepsilon_{\beta\rho\sigma}\sum_{k,\nu_k}\left[\frac{\langle g\nu_g|T_{\alpha\rho}^{+}|k\nu_k\rangle\langle k\nu_k|\mu_o^p|f\nu_f\rangle}{\omega_{k\nu_k} - \omega} + \frac{\langle g\nu_g|\mu_o^p|k\nu_k\rangle\langle k\nu_k|T_{\alpha\rho}^{+}|f\nu_f\rangle}{\omega_{k\nu_k} - \omega}\right] \quad (13) $$

Here, the summations run over all the intermediate electronic ($|k\rangle$) and vibrational ($|\nu_k\rangle$) states. $\varepsilon_{\alpha\beta\gamma}$ is the Levi Civita alternating tensor, and μ_α^p is the α component of the dipole velocity operator, defined as

$$ \mu_\alpha^p = \sum_i \frac{q_i}{m_i} p_{i\alpha} \quad (14) $$

and $T_{\alpha\beta}^{+}$ is the $\alpha\beta$ component of the mixed length−velocity form of the quadrupole operator

$$ T_{\alpha\beta}^{+} = \sum_i \frac{q_i}{m_i}(p_{i\alpha} r_{i\beta} + r_{i\alpha} p_{i\beta}) \quad (15) $$

Because the optical photon frequency ω is far larger than any of the excitation energies of the vibrational states contributing significantly to the summation, we can assume $\omega_{k\nu_k} \cong \omega_k$. Therefore, using the closure relationship $\sum_{\nu_k}|\nu_k\rangle\langle\nu_k| = 1$, in eq 11

$$ P_{\alpha\beta}^{p,g\nu_g f\nu_f}(\omega) = \langle \nu_g|P_{\alpha\beta}^{p,e}(\omega, \boldsymbol{Q})|\nu_f\rangle \quad (16) $$

where $P_{\alpha\beta}^{p,g}(\omega, \boldsymbol{Q})$ is the electronic (vertical-transition) tensor

$$ P_{\alpha\beta}^{p,e}(\omega, \boldsymbol{Q}) = \sum_k\left[\frac{\langle g|\mu_\alpha^p|k\rangle\langle k|\mu_\beta^p|f\rangle}{\omega_k - \omega} + \frac{\langle g|\mu_\beta^p|k\rangle\langle k|\mu_\alpha^p|f\rangle}{\omega_k - \omega}\right] \quad (17) $$

and the summation includes the ground state $|g\rangle$. The explicit dependence of $P_{\alpha\beta}^{p,g}(\omega, \boldsymbol{Q})$ on the photon frequency introduces a severe complication with respect to the case of one-photon absorption.[21] A very useful approximation is to compute $P_{\alpha\beta}^{p,e}(\omega_0, \boldsymbol{Q})$, the transition moment at the fixed photon frequency ω_0, corresponding to the two-photon vertical excitation (which roughly coincides with the maximum of the intensity). In this approach, the dependence on the spectrum on the frequency is introduced by the $g(2\omega, \omega_{g\nu_g f\nu_f})$ line shape weighted by the rotatory strengths ${}^{g\nu_g f\nu_f}R_{\mathrm{TPCD}}$ and by the ω^2 prefactor, as seen in eq 6. Such an approximation may fail when resonances (or nearby resonances) exist with specific vibronic levels. Inspection of the electronic energy levels (see footnote of Table 1) allows us to exclude this possibility in our application to R3MCP, vide infra. Expanding $P_{\alpha\beta}^{p,g}(\omega_0, \boldsymbol{Q})$ in a Taylor series with respect to the normal coordinates of the ground electronic state ${}^g\boldsymbol{Q}$ around the equilibrium geometry ${}^g\boldsymbol{Q}_0$, we have

$$ P_{\alpha\beta}^{p,e}(\omega_0, {}^g\boldsymbol{Q}) = P_{\alpha\beta}^{p,e}(\omega_0, {}^g\boldsymbol{Q}_0) + \sum_a \frac{\partial P_{\alpha\beta}^{p,e}(\omega_0, {}^g\boldsymbol{Q})}{\partial {}^gQ_a} {}^gQ_a + \ldots \quad (18) $$

and therefore in the limit of first-order expansion we have

$$ P_{\alpha\beta}^{p,g\nu_g f\nu_f}(\omega_0) = P_{\alpha\beta}^{p,e}(\omega_0, {}^g\boldsymbol{Q}_0)\langle \nu_g|\nu_f\rangle + \sum_a \frac{\partial P_{\alpha\beta}^{p,e}(\omega_0, {}^g\boldsymbol{Q})}{\partial {}^gQ_a}\langle \nu_g|{}^gQ_a|\nu_f\rangle \quad (19) $$

The first quantity on the right-end side is the electronic transition moment of the initial state at the equilibrium position of the ground electronic state, multiplied by the FC overlap. The second term arises from the vibronic coupling between different electronic states, and it yields the so-called HT contribution. The expressions for the tensors defined in eqs 12 and 13 are obtained from eq 19 by substituting P^p with M^p and T^+, respectively.

The extinction coefficient in TPA is defined as[43]

$$ \delta^{\mathrm{TPA}}(\omega) = \frac{1}{30}\frac{(2\pi)^2 \times \omega^2 \times N_{\mathrm{A}}}{c_0^2 \times (4\pi\varepsilon_0)^2} \times \sum_f \sum_{\nu_g,\nu_f} p_{\nu_g} g(2\omega, \omega_{g\nu_g f\nu_f}) \times {}^{g\nu_g f\nu_f}\delta_{\mathrm{TPA}}(\omega_0) \approx 8.00460 \times 10^{-31} \times \omega^2 \times \sum_f \sum_{\nu_g,\nu_f} p_{\nu_g} g(2\omega, \omega_{g\nu_g f\nu_f}) \times {}^{g\nu_g f\nu_f}\delta_{\mathrm{TPA}}(\omega_0) \quad (20) $$

The orientationally averaged two-photon probability ${}^{g\nu_g f\nu_f}\delta_{\mathrm{TPA}}(\omega_0)$ is given by

$$ {}^{g\nu_g f\nu_f}\delta_{\mathrm{TPA}}(\omega_0) = \sum_{\alpha\beta}(F \times S_{\alpha\alpha}^{g\nu_g f\nu_f} S_{\beta\beta}^{*,g\nu_g f\nu_f} + G \times S_{\alpha\beta}^{g\nu_g f\nu_f} S_{\alpha\beta}^{*,g\nu_g f\nu_f} + H \times S_{\alpha\beta}^{g\nu_g f\nu_f} S_{\beta\alpha}^{*,g\nu_g f\nu_f}) \quad (21) $$

where $S_{\alpha\beta}^{g\nu_g f\nu_f}$ is the two-photon transition matrix element

$$S_{\alpha\beta}^{g\nu_g f\nu_f}(\omega_0) = \frac{1}{\hbar}\sum_{k,\nu_k}\left[\frac{\langle g\nu_g|\mu_\alpha|k\nu_k\rangle\langle k\nu_k|\mu_\beta|f\nu_f\rangle}{\omega_{k\nu_k}-\omega_0} + \frac{\langle g\nu_g|\mu_\beta|k\nu_k\rangle\langle k\nu_k|\mu_\alpha|f\nu_f\rangle}{\omega_{k\nu_k}-\omega_0}\right] \quad (22)$$

and F, G, and H assume values of 2, 2, 2 for linearly and −2, 3, 3 for circularly polarized beams, respectively. We can write

$$S_{\alpha\beta}^{g\nu_g f\nu_f}(\omega_0) = S_{\alpha\beta}^{e}(\omega_0, {}^g\boldsymbol{Q}_0)\langle\nu_g|\nu_f\rangle + \sum_a \frac{\partial S_{\alpha\beta}^{e}(\omega_0, {}^g\boldsymbol{Q})}{\partial {}^gQ_a}\langle\nu_g|{}^gQ_a|\nu_f\rangle \quad (23)$$

where $S_{\alpha\beta}^{e}$ is the corresponding electronic two-photon absorption tensor, obtained from eq 17 upon substitution of P^p with S.

The last rows of eqs 6 and 20 yield the TPCD and TPA in units of cm^4 sec mol^{-1} starting from circular frequencies, two-photon rotatory strengths, and transition probabilities given in atomic units. By dividing by Avogadro's number and by multiplying by 10^{50}, the observables can be obtained in often used units of GM (Göppert−Mayer).

2.2. Analytical Sum Rules for Total Intensity. Similar to what we have done for ECD,[21] we can derive analytical sum rules for the total intensity of TPCD. We neglect the frequency-dependence, and to that end, for each transition $|g\nu_g\rangle \rightarrow |f\nu_f\rangle$, we define the three terms $\bar{B}_i^{\mathrm{TI}}(\omega_0) = \omega^3 B_i^{\mathrm{TI}}(\omega_0)$, where $i = 1, 2, 3$ and the quantities $B_i^{\mathrm{TI}}(\omega)$ are given in eqs 8−10. In the limit of first-order expansions of the three tensors defined in eqs 11, 12, and 13 and assuming completeness of the vibrational-state manifold, we have

$$\begin{aligned}\sum_{\nu_g,\nu_f}\bar{B}_1^{\mathrm{TI}}(\omega_0) &= \sum_{\rho\sigma}\sum_{\nu_g,\nu_f} p_{\nu_g}\langle\nu_g|M_{\rho\sigma}^{p,e}(\omega_0, {}^g\boldsymbol{Q})|\nu_f\rangle\langle\nu_f|P_{\rho\sigma}^{p,e}(\omega_0, {}^g\boldsymbol{Q})|\nu_g\rangle \\ &= \sum_{\rho\sigma}\sum_{\nu_g} p_{\nu_g}\langle\nu_g|M_{\rho\sigma}^{p,e}(\omega_0, {}^g\boldsymbol{Q})P_{\rho\sigma}^{p,e}(\omega_0, {}^g\boldsymbol{Q})|\nu_g\rangle \\ &= \sum_{\rho\sigma}\sum_{\nu_g} p_{\nu_g}\langle\nu_g|\left[M_{\rho\sigma}^{p,e}(\omega_0, {}^g\boldsymbol{Q}_0) + \sum_a \frac{\partial M_{\rho\sigma}^{p,e}(\omega_0, {}^g\boldsymbol{Q})}{\partial {}^gQ_a}{}^gQ_a\right] \\ &\quad \left[P_{\rho\sigma}^{p,e}(\omega_0, {}^g\boldsymbol{Q}_0) + \sum_b \frac{\partial P_{\rho\sigma}^{p,e}(\omega_0, {}^g\boldsymbol{Q})}{\partial {}^gQ_b}{}^gQ_b\right]|\nu_g\rangle \\ &= \sum_{\rho\sigma}\left[M_{\rho\sigma}^{p,e}(\omega_0, {}^g\boldsymbol{Q}_0)P_{\rho\sigma}^{p,e}(\omega_0, {}^g\boldsymbol{Q}_0) + \sum_a\sum_{\nu_g} p_{\nu_g}\frac{\partial M_{\rho\sigma}^{p,e}(\omega_0, {}^g\boldsymbol{Q})}{\partial {}^gQ_a}\frac{\partial P_{\rho\sigma}^{p,e}(\omega_0, {}^g\boldsymbol{Q})}{\partial {}^gQ_a}\frac{\hbar}{2\omega_a}(2\nu_{a,g}+1)\right] \\ &= \bar{\mathrm{B}}_1^{\mathrm{TI,FC}} + \bar{\mathrm{B}}_1^{\mathrm{TI,HT}} \end{aligned} \quad (24)$$

Analogously, we can prove that the following hold

$$\begin{aligned}\sum_{\nu_g,\nu_f}\bar{B}_1^{\mathrm{TI}}(\omega_0) &= \frac{1}{2}\sum_{\rho\sigma}\left[T_{\rho\sigma}^{+,e}(\omega_0, {}^g\boldsymbol{Q}_0)P_{\rho\sigma}^{p,e}(\omega_0, {}^g\boldsymbol{Q}_0) + \sum_a\sum_{\nu_g} p_{\nu_g}\frac{\partial T_{\rho\sigma}^{+,e}(\omega_0, {}^g\boldsymbol{Q})}{\partial {}^gQ_a}\frac{\partial P_{\rho\sigma}^{p,e}(\omega_0, {}^g\boldsymbol{Q})}{\partial {}^gQ_a}\frac{\hbar}{2\omega_a}(2\nu_{a,g}+1)\right] \\ &= \bar{\mathrm{B}}_2^{\mathrm{TI,FC}} + \bar{\mathrm{B}}_2^{\mathrm{TI,HT}} \end{aligned} \quad (25)$$

$$\begin{aligned}\sum_{\nu_g,\nu_f}\bar{B}_3^{\mathrm{TI}}(\omega_0) &= \sum_{\rho\sigma}\left[M_{\rho\rho}^{p,e}(\omega_0, {}^g\boldsymbol{Q}_0)P_{\sigma\sigma}^{p,e}(\omega_0, {}^g\boldsymbol{Q}_0) + \sum_a\sum_{\nu_g} p_{\nu_g}\frac{\partial M_{\rho\rho}^{p,e}(\omega_0, {}^g\boldsymbol{Q})}{\partial {}^gQ_a}\frac{\partial P_{\sigma\sigma}^{p,e}(\omega_0, {}^g\boldsymbol{Q})}{\partial {}^gQ_a}\frac{\hbar}{2\omega_a}(2\nu_{a,g}+1)\right] \\ &= \bar{\mathrm{B}}_3^{\mathrm{TI,FC}} + \bar{\mathrm{B}}_3^{\mathrm{TI,HT}} \end{aligned} \quad (26)$$

Therefore, the total intensity of the TPCD rotatory strength can be written as

$$\begin{aligned}\sum_{\nu_g,\nu_f}{}^{g\nu_g f\nu_f}\bar{R}^{\mathrm{TP}} &= (-b_1\bar{\mathrm{B}}_1^{\mathrm{TI,FC}} - b_2\bar{\mathrm{B}}_2^{\mathrm{TI,FC}} - b_3\bar{\mathrm{B}}_3^{\mathrm{TI,FC}}) + (-b_1\bar{\mathrm{B}}_1^{\mathrm{TI,HT}} - b_2\bar{\mathrm{B}}_2^{\mathrm{TI,HT}} - b_3\bar{\mathrm{B}}_3^{\mathrm{TI,HT}}) \\ &= \bar{\mathrm{R}}_{\mathrm{TPCD}}^{\mathrm{FC}} + \bar{\mathrm{R}}_{\mathrm{TPCD}}^{\mathrm{HT}} \end{aligned} \quad (27)$$

The corresponding expression for the analytical total intensity for TPA reads as

$$\begin{aligned}\sum_{\nu_g,\nu_f}{}^{g\nu_g f\nu_f}\delta_{\mathrm{TPA}}(\omega_0) &= \sum_{\rho\sigma}[F\times S_{\rho\rho}^{e}(\omega_0, {}^g\boldsymbol{Q}_0)S_{\sigma\sigma}^{e,*}(\omega_0, {}^g\boldsymbol{Q}_0) + G\times S_{\rho\sigma}^{e}(\omega_0, {}^g\boldsymbol{Q}_0)S_{\rho\sigma}^{e,*}(\omega_0, {}^g\boldsymbol{Q}_0) + H\times S_{\rho\sigma}^{e}(\omega_0, {}^g\boldsymbol{Q}_0)S_{\sigma\rho}^{e,*}(\omega_0, {}^g\boldsymbol{Q}_0)] + \\ &\quad \sum_a\sum_{\nu_g} p_{\nu_g}\frac{\hbar}{2\omega_a}(2\nu_{a,g}+1)\left[F\times\frac{\partial S_{\rho\rho}^{e}(\omega_0, {}^g\boldsymbol{Q})}{\partial {}^gQ_a}\frac{\partial S_{\sigma\sigma}^{e,*}(\omega_0, {}^g\boldsymbol{Q})}{\partial {}^gQ_a} + G\times\frac{\partial S_{\rho\sigma}^{e}(\omega_0, {}^g\boldsymbol{Q})}{\partial {}^gQ_a}\frac{\partial S_{\rho\sigma}^{e,*}(\omega_0, {}^g\boldsymbol{Q})}{\partial {}^gQ_a} + H\times\frac{\partial S_{\rho\sigma}^{e}(\omega_0, {}^g\boldsymbol{Q})}{\partial {}^gQ_a}\frac{\partial S_{\sigma\rho}^{e,*}(\omega_0, {}^g\boldsymbol{Q})}{\partial {}^gQ_a}\right] = \delta_{\mathrm{TPA}}^{\mathrm{FC}} + \delta_{\mathrm{TPA}}^{\mathrm{HT}} \end{aligned} \quad (28)$$

Eq 28 generalizes for finite temperature and both linear and circular polarized light the 0 Kelvin expression, obtained for linear-polarized light only, by Macák et al.[33]

3. Computational Details

Attention is focused here on the two lowest-lying conformers identified for gaseous R3MCP, the so-called equatorial-methyl (*Eq*) and axial-methyl (*Ax*) forms, whose structures are also sketched in the inset of Figure 1. The optimized geometries, the normal modes and the corresponding frequencies of the electronic ground-state are taken from ref 20. They were obtained at DFT level based on the hybrid Becke three parameters Lee−Yang−Parr (B3LYP) functional,[44−46] adopting the aug-cc-pVTZ basis set[47] and using *Gaussian 03*.[48]

The $P_{\alpha\beta}^{p,g\nu_g f\nu_f}(\omega)$, $M_{\alpha\beta}^{p,g\nu_g f\nu_f}(\omega)$, $T_{\alpha\beta}^{+,g\nu_g f\nu_f}(\omega)$, and $S_{\alpha\beta}^{g\nu_g f\nu_f}(\omega)$ tensors were evaluated as single residues of the appropriate quadratic response functions,[6] using the *DALTON 2.0* chemistry program.[49] Their derivatives with respect to normal coordinates were obtained by numerical differentiation.

In the property calculations, we employed the Coulomb-attenuated Becke three parameters Lee−Yang−Parr (CAM-B3LYP) functional,[50,51] which in our previous study of the ECD spectra[19−21] yielded a considerable improvement with respect to results obtained with the popular hybrid B3LYP functional. In our calculations, performed with the aug-cc-pVTZ basis set, the standard parametrization ($\alpha = 0.190$, $\beta = 0.460$, $\mu = 0.330$) was used for CAM-B3LYP.

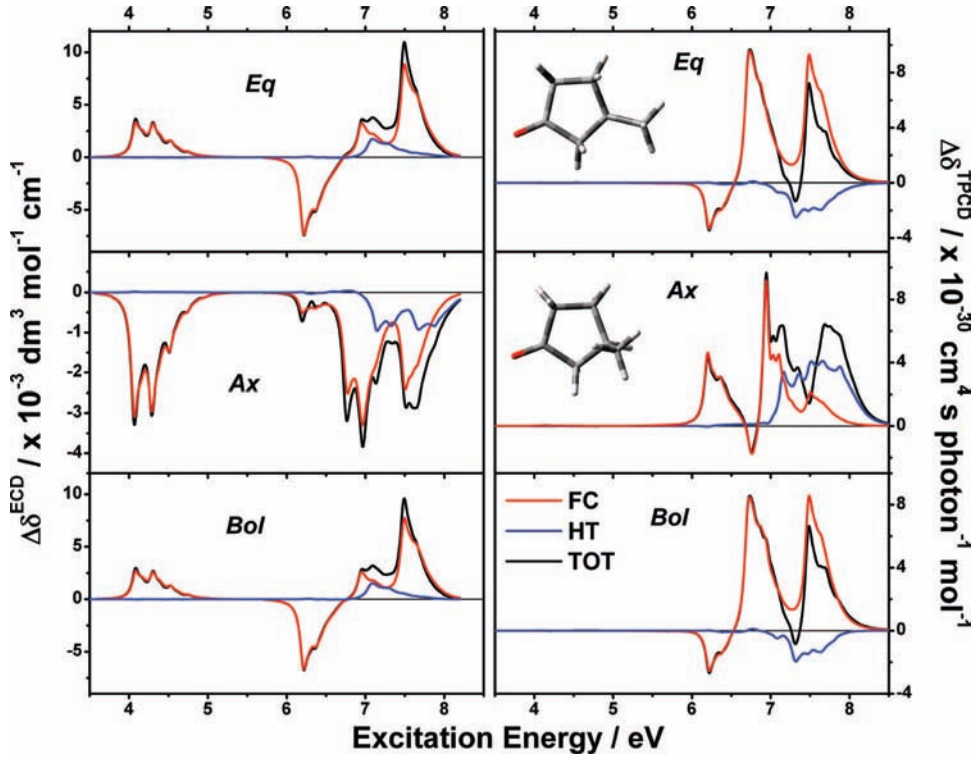

Figure 1. Vibronically resolved one- (ECD, left panels) and two- (TPCD, right panels) photon circular dichroism spectra of the equatorial-methyl (*Eq*) and axial-methyl (*Ax*) conformers of R3MCP. The Boltzmann-averaged (*Bol*) spectra are also shown. The linear coupling vibronic model (LCM) is employed. CAM-B3LYP/aug-cc-pVTZ property calculations carried out on ground-state B3LYP/aug-cc-pVTZ optimized geometries, in the energy interval where our calculations place the first six excited electronic states. Franck−Condon (FC, red lines) and Herzberg−Teller (HT, blue lines) contributions, together with the total (TOT = FC + HT, black lines) spectra are shown with a Lorentzian broadening of 0.05 eV.

TABLE 1: Analytical Franck−Condon (FC) and Herzberg−Teller (HT) Total Intensities and Convergence (%, See Text for the Definition; in Parentheses the Harmonic AFC Values Are Given) for the LCM Calculation of the TPCD Responses of Both the Equatorial (*Eq*) and Axial (*Ax*) Conformers of R3MCP[a,b]

	Total Intensities				Convergence					
	Eq		*Ax*		*Eq*			*Ax*		
	FC	HT	FC	HT	FC	HT	TOT	FC	HT	TOT
S1	−0.0001	0.0003	0.0008	−0.0004	100 (99.8)	99.8 (99.1)	100 (99.4)	100 (99.8)	99.6 (99.3)	99.7 (100)
S2	−0.1069	−0.0041	0.1404	0.0021	100 (99.9)	99.5 (99.6)	99.9 (99.9)	100 (99.8)	99.7 (98.8)	100 (99.8)
S3	0.3817	0.0032	−0.1066	0.0017	99.9	104	99.9	99.9	96.4	99.8
S4	−0.0203	−0.0650	0.5823	−0.1496	100	99.6	99.9	100	99.5	100
S5	−0.0066	−0.0294	−0.3056	0.2930	100	99.8	99.8	100	99.9	103
S6	0.3620	−0.0670	0.0774	0.2668	100	99.5	100	100	99.3	99.2

[a] First six excited states, calculated at the CAM-B3LYP/aug-cc-pVTZ level. Atomic units. [b] The S0 → S*n* (*n* = 1,6) vertical excitation energies (eV) are 4.30, 6.33, 6.86, 7.03, 7.06, and 7.61 for the *Eq* conformer and 4.28, 6.32, 6.89, 7.06, 7.08, and 7.63 for the *Ax* conformer, respectively.

The Boltzmann averaging of the spectra was carried out at 298.15 K and 1 atm, as detailed in refs 19−21. The Boltzmann percentages of the two conformers in the gas phase computed at B3LYP/aug-cc-pVTZ level were 89.9% and 10.1%, for the *Eq* and *Ax* forms, respectively.[21]

All of the spectra reported in this work were computed with a modified version of the code *FCclasses*.[52] The program was generalized to deal with second-rank two-photon transition tensors. Furthermore, the selection scheme of the vibronic transitions presented in ref 28 was slightly modified to take into account and balance the HT contributions of the three different transition tensors in eqs 11−13. Following what we have done for ECD,[21] harmonic AFC spectra were obtained for the first two excited states for OPA, TPA, and TPCD processes. We resorted to the less-expensive LCM to study the response of the S3−S6 excited states, and we compared LCM and AFC results for the S1 and S2 states. LCM spectra are computed at CAM-B3LYP/aug-cc-pVTZ level on the B3LYP/aug-cc-pVTZ geometries for both conformers. For the S1 and S2 harmonic AFC spectra, we utilized the excited states optimized geometries and harmonic analyses obtained in ref 21 at the TD-DFT CAM-B3LYP/aug-cc-pVDZ level, exploiting the analytical gradients available in the development version of the *Gaussian* computational package.[53] The excited-state energy minima were refined at the CAM-B3LYP/aug-cc-pVTZ level for both conformers. The possible effect on the shape of our spectra of the S1 anharmonic double-well energy profile along the pyramidalization mode of the carbonylic C was discussed in detail in ref 21, and it is treated approximately here, following the same procedure described thereof.

4. Results and Discussion

4.1. Comparison of TPCD and ECD Spectra Computed at the LCM Level. Figure 1 shows vibronically resolved one- (left panels) and two- (right panels) photon circular dichroism

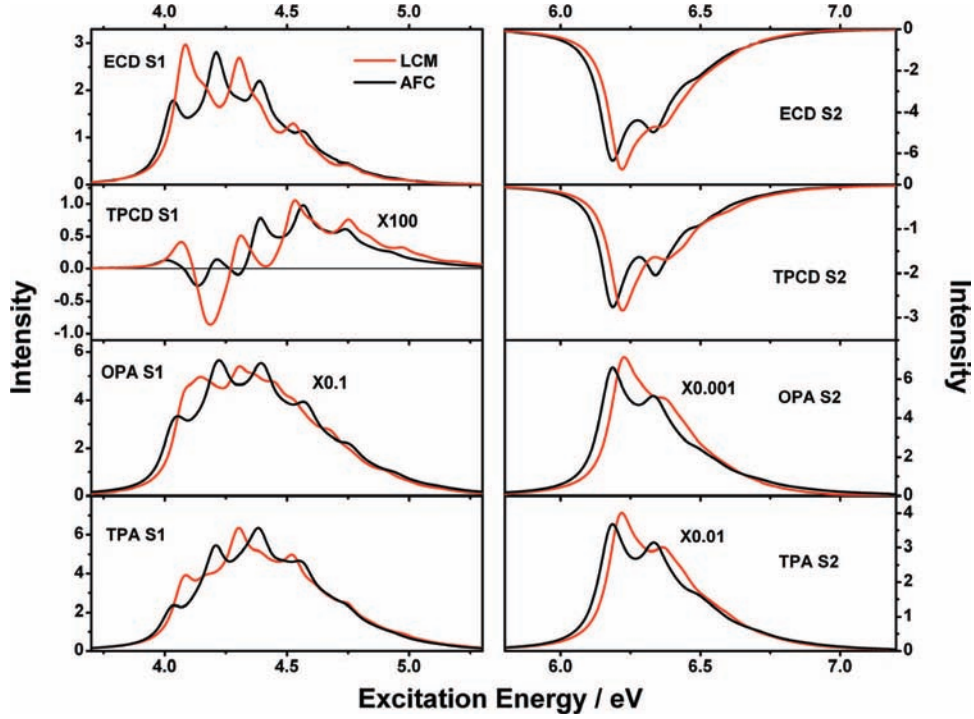

Figure 2. Boltzmann-averaged one- (ECD, eq 1) and two- (TPCD, eq 6) photon circular dichroism, one- (OPA, eq 5) and two- (TPA, eq 20) photon absorption spectra for the S1 and S2 states of R3MCP, computed at the CAM-B3LYP/aug-cc-pVTZ level and obtained with the linear coupling (LCM, red lines) and the Harmonic AFC (AFC, black lines) models. All spectra are convoluted with a Lorentzian broadening of 0.05 eV. The units are: 10^{-3} dm^3 mol^{-1} cm^{-1} for both ECD and OPA; 10^{-30} cm^4 s photon^{-1} mol^{-1} for both TPCD and TPA.

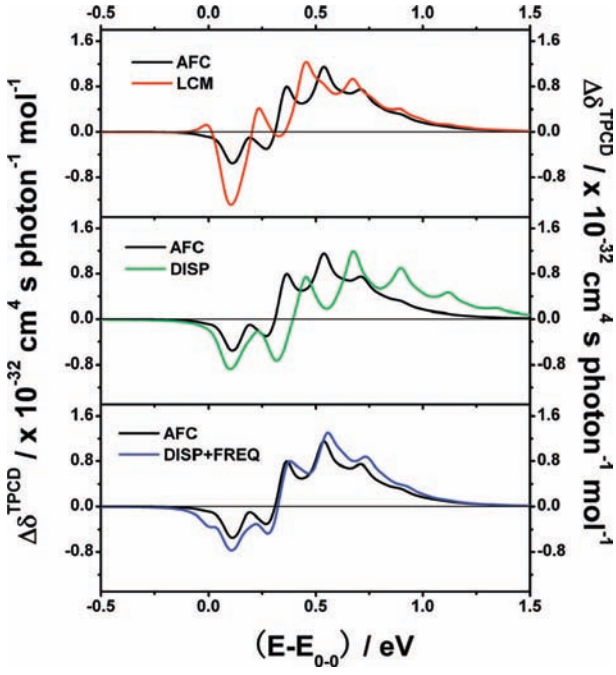

Figure 3. Comparison between two-photon circular dichroism (TPCD) spectrum for the first (S1) excited-state computed by Harmonic AFC (AFC, black line) and by a independent-mode model as LCM (red line). The green curve "DISP" in the middle panel reports the independent-mode prediction employing the AFC displacements and the LCM values for excited-state frequencies; the blue curve "DISP+FREQ" in the bottom panel is obtained with the independent-mode model adopting AFC values both for the frequencies and the displacements. The spectrum is given as a function of $(E-E_{0,0})$, unit of eV, where E is the excitation energy and $E_{0,0}$ is the 0−0 transition energy.

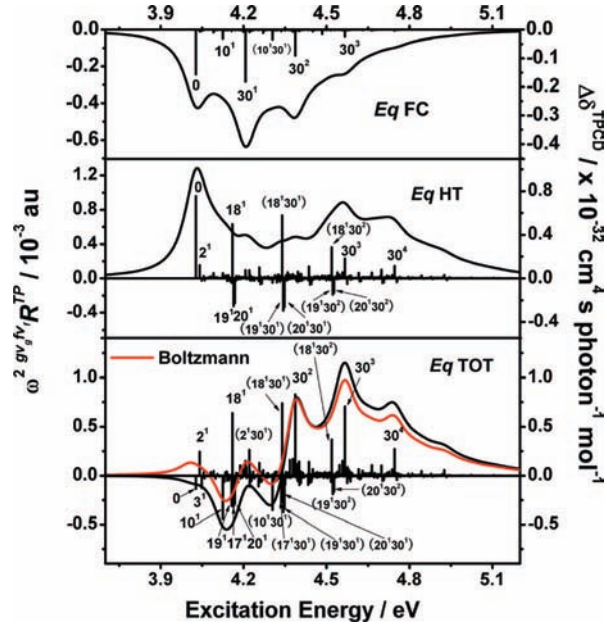

Figure 4. Assignments of the main stick bands of the Franck−Condon (FC, top panel), Herzberg−Teller (HT, middle panel), and total (TOT = FC+HT, bottom panel) vibronic spectra for the *Eq* conformer of R3MCP in the S1 region, as obtained with the Harmonic AFC (AFC) model. Vibrational contributions are labeled as "n^x", where x indicates the quanta deposited on the excited-state normal mode n. When the x is not explicitly given, it is intended that the corresponding mode is in the ground state ($x = 0$). Combination bands, $n^x m^y$, are indicated in parentheses. The spectra are convoluted with a Lorentzian spectral shape function with a broadening of 0.05 eV. The Boltzmann-averaged spectrum is also shown in red.

spectra of the *Eq* and *Ax* conformers of R3MCP, obtained employing the LCM, in the region of wavelengths where the first six excited electronic states are placed by our calculations. The Boltzmann-averaged (*Bol*, $T = 298.15$ K, $P = 1$ atm) spectra are also shown. FC (red lines) and HT (blue lines) contributions, together with the total spectra (TOT = FC + HT,

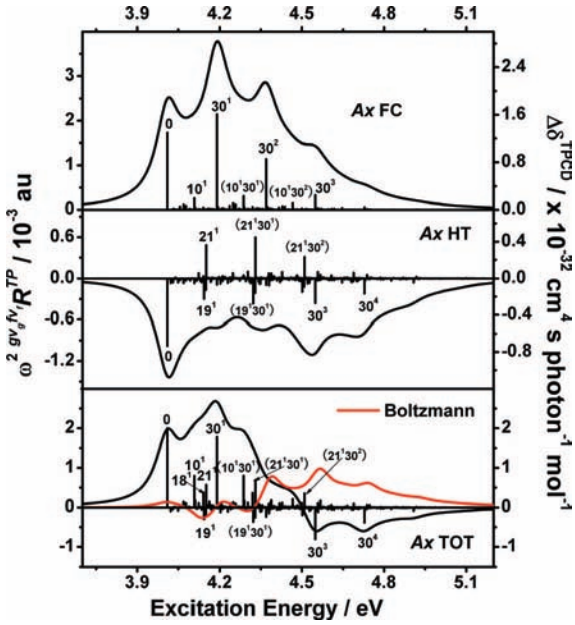

Figure 5. Assignments of the main stick bands of the Franck−Condon (FC, top panel), Herzberg−Teller (HT, middle panel), and total (TOT, bottom panel) vibronic spectra for the *Ax* conformer of R3MCP in the S1 region, as obtained with the Harmonic AFC (AFC) model. Vibrational contributions are labeled as "n^x", where x indicates the quanta deposited on the excited-state normal mode n. When the x is not explicitly given, it is intended that the corresponding mode is in the ground state ($x = 0$). Combination bands, $n^x m^y$, are indicated in parentheses. The spectra are convoluted with a Lorentzian spectral shape function with a broadening of 0.05 eV. The Boltzmann-averaged spectrum is also shown in red.

TABLE 2: Franck−Condon (FC), Herzberg−Teller (HT), and Total (TOT) Intensities of Some Selected Vibronic Transitions for Two-Photon Circular Dichroism (TPCD) Responses of Both the Equatorial (*Eq*) and Axial (*Ax*) Conformers of R3MCP, for the First Excited State, Calculated with the Harmonic AFC Vibronic Model; Atomic Units (10^{-3} au)

	Eq			*Ax*		
	FC	HT	TOT	FC	HT	TOT
$0-0$	−0.242	0.959	−0.136	1.726	−0.979	1.998
10^1	−0.048	0.059	−0.445	0.262	−0.069	0.794
30^1	−0.283	0.094	0.148	2.145	−0.091	1.780
$10^1 30^1$	−0.053	−0.046	−0.351	0.306	0.043	0.796
30^2	−0.141	0.030	0.827	1.139	−0.095	−0.235
30^3	−0.038	0.232	0.705	0.329	−0.361	−0.803
30^4	−0.006	0.143	0.270	0.054	−0.223	−0.384

black lines) are convoluted with an experimentally reasonable Lorentzian broadening of 0.05 eV. The vibronically resolved ECD spectra were already presented and discussed in detail in ref 21, also ref 20, and they are reported here for ease of comparison.

Figure 1 shows that R3MCP gives rather different one- and two-photon responses. The first excited state, S1, is ECD active but it shows very weak TPCD signals for both conformers. The second excited state, S2, displays negative peaks for both *Eq* and *Ax* (the latter a bit less intense than the former) in ECD, whereas for TPCD the sign is negative for *Eq* and positive for *Ax*. The S3−S6 states, which are very close in energy, yield together a positive signal in *Eq* and a negative one in *Ax* for ECD. The TPCD signal is instead a succession of peaks of different sign, both for the *Eq* and the *Ax* conformers. Further details can be found in ref 19. The *Eq* conformer largely dominates in the Boltzmann-averaged spectra due to the ∼9:1 ratio coming from the thermal distribution.

4.2. Analysis of TPCD Total Intensities. A very convenient way to compare the relevance of FC and HT contributions is through the total intensities (section 2.2). Note however that the HT effect on the spectrum profile may be ill-estimated by an analysis of its analytical sum only, because HT contributions may in principle be positive or negative. In Table 1, we collect the TPCD analytical sum of the FC and HT total intensities, for both *Eq* and *Ax* conformers, postponing to section 4.3 a detailed analysis on S1 for both conformers because the signal due to this state is too weak to be seen on the scale of Figure 1. The ECD spectrum was analyzed in detail in our previous study,[21] also see ref 20. For the *Eq* conformer, as we can clearly see in Figure 1, the FC contributions dominate for both S2 and S3, being responsible for the negative and positive peak around 6.20 and 6.73 eV, respectively. This is consistent with the contents of Table 1, where the total FC intensity is found to be much larger than the corresponding total analytical HT intensity, cf. ratios FC/HT = 26 and 119 for S2 and S3, respectively. There are HT contributions arising in the S4−S6 region, whose effects on the TOT spectrum are visible in this area. Indeed, for S4 and S5 the HT signal becomes even larger than the corresponding FC contribution, with ratios of FC/HT = 0.3 and 0.2, respectively. A similar conclusion can be drawn for *Ax*. The HT contributions become important in the S4−S6 region, those of S4 and S5 being comparable and yet still smaller than those of FC, whereas HT is larger than FC for S6, with a ratio FC/HT = 0.3.

This analysis shows that in R3MCP HT effects are remarkable even for the transitions responsible for the strongest signals, suggesting that a theory including only FC effects may be more often inadequate for TPCD than for one-photon processes. Notice nevertheless that S3, S4, and S5 were identified in ref 19 as members of a close-lying multiplet of $n \rightarrow 3p$ character, whereas S6 appears to be the lowest-lying member of the corresponding $n \rightarrow 3d$ manifold. The adiabatic HT approach employed in this study might then not fully describe the details of the vibronic borrowing mechanism, and in particular the effect of the missing members of the $n \rightarrow 3d$ multiplet might change the shape of the spectra in upper energy range, above ∼6.5 eV. On the other hand, a fully nonadiabatic multistate description of the TPCD signal, including the possibility of occurrences of conical intersections, is currently unfeasible.

In Table 1, we collect also information on the convergence over the vibronic manifold of our TPCD calculations. For each final state, this convergence is estimated as the ratio between the sum of the intensities of the state-to-state rotatory strength, eq 7, explicitly considered in the computation of the spectrum (taking into account both the FC and the HT contributions (TOT), or each of them separately) and the corresponding total analytical intensities. In parentheses in Table 1, the harmonic AFC values are given. Very satisfactory levels of convergence are obtained for both FC and HT, both with the LCM and harmonic AFC vibronic models. The convergence is excellent also for TOT, to a level always intermediate between those of the FC and HT contributions, even when large cancellations between FC and HT make the calculation rather challenging. Notice that because vibronic circular dichroism intensities can be either positive or negative, the sum of the state-to-state intensities included in the spectrum is not bound to converge to the analytical sum from below (which explains ratios larger than 100% in Table 1).

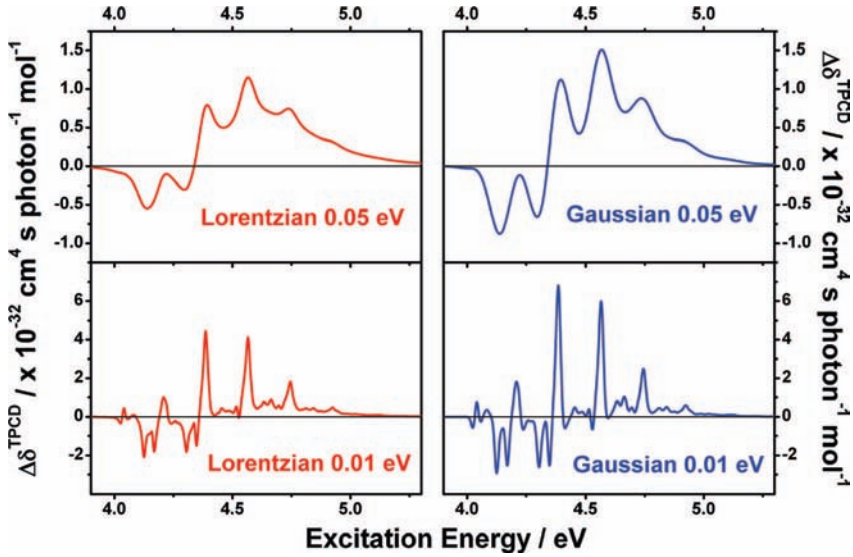

Figure 6. Profile of the AFC TPCD spectrum of the equatorial conformer of R3MCP in the region where the S1 state is active, resulting from the choice of either Gaussian (in blue) or Lorentzian (in red) line shapes and with two different HWHM (half width at half-maximum), 0.01 and 0.05 eV, respectively.

4.3. AFC Spectra for S1 and S2 States. Comparison of OPA, TPA, ECD, and TPCD Signals. An experimental ECD spectrum recorded at photon energies falling in the range where the first two excited states, S1 and S2, lie was reported for instance in refs 31 and 32. With the aim of providing as precise as possible vibrational assignments of the main experimental peaks, in ref 21 we went beyond the LCM and computed the Harmonic AFC ECD spectra for S1 and S2, including both frequency changes and Duschinsky rotation of the normal modes. Here, we apply the same strategy for two-photon absorption and dichroism processes. In Figure 2, we report the computed Boltzmann-averaged OPA, eq 5; ECD, eq 1; TPA, eq 20; and TPCD, eq 6 spectra of R3MCP in the S1−S2 region as obtained with the AFC vibronic model. The LCM spectra are also shown for comparison. Data in Table 1 show that full converged vibronic spectra have been obtained both at LCM and AFC levels.

At the Franck−Condon level, all of the four spectra (OPA, ECD, TPA, and TPCD) are expected to yield the same shape because the relative heights (progressions) of the vibrational bands depend only on the FC factors, and they are uniquely determined for two given states of the system. The differences in shape between spectra of different properties are due to HT effects. Minor differences are seen in the shape of the four signals deriving from the S2 state (apart from the overall sign, negative for CD). The ECD, OPA, and TPA S1 signals are rather similar, with a moderate enhancement (from ECD to TPA) of the blue vibrational peaks, mainly due to a progression along the normal mode 30 corresponding to the C=O stretch.

The S1 TPCD shape is strikingly different from the other three signals as a result of the dominance of HT contributions. Therefore, this case will be investigated in detail below because it represents an interesting playground to analyze the possible combined HT and Duschinsky effects at work.

Figure 2 shows that LCM and AFC yield rather similar spectra for S2 for all computed properties, except for a small blue-shift of the LCM peaks with respect to the AFC ones. This shift originates from the overestimation of the calculated adiabatic energy difference between the minima of the S1 and S0 states. More significant differences can be found in the S1 region, most likely due to its $n \rightarrow \pi^*$ character, as already discussed in ref 21. Again we postpone the discussion on TPCD, and note that for the other three signals the LCM/AFC difference in the relative heights of the peaks is mainly due to the different estimate of the initial and final-state equilibrium geometry displacements by the two models. These are underestimated to a larger extent by LCM (notice that for ECD the AFC model provides a better agreement with the experiment[21]). The difference in the spacing between the peaks is due to the overestimation of the excited-state frequencies by LCM.

In Figure 3, we present a detailed comparison between LCM and AFC spectra for the rather complicate TPCD response of the S1 state of the dominant *Eq* conformer (a similar comparison could be done for the other three spectra). The spectra are plotted vis the relative energies with respect to the 0−0 transition energy, $E_{0,0}$. The latter is set to zero, to remove the trivial differences due to different estimates of adiabatic energy difference. The top panel of Figure 3 shows that LCM (red line) predicts a significantly different vibrational structure with respect to AFC (black line), especially in the region where the sign inversion takes place: two negative peaks in AFC are replaced by a single one in LCM. LCM is an independent-mode model, contrary to AFC where modes are mixed by Duschinsky couplings. Beyond the latter, there are two other possible causes for the difference of the LCM and AFC predictions: frequencies and displacements. In fact, AFC and LCM differ for the estimated values of the frequencies of the excited state, that are computed by harmonic analysis of the excited-state PES in AFC, whereas they are taken equal to those of the ground-state in LCM. Additionally, LCM and AFC differ for the estimate of the displacements between the equilibrium structures of the initial and final states. In the LCM, these are computed from the excited-state energy gradient at the ground-state geometry (exploiting the assumption of equal frequencies for the ground and excited state), whereas AFC obtains them directly from a geometry optimization of the excited state.

To rationalize the role played by displacements, frequencies and Duschinsky mixings in determining the LCM/AFC difference, we performed a step-by-step comparison considering a harmonic independent-mode model as LCM and modifying progressively its parameters, displacements, and excited-state frequencies, setting them equal to those adopted by AFC. The green curve "DISP" in the middle panel of Figure 3 reports the independent-mode

prediction employing the AFC displacements and the LCM values for excited-state frequencies; the blue curve "DISP+FREQ" in the lower panel of Figure 3 is obtained with the independent-mode model adopting AFC values both for the frequencies and the displacements. Inspection of the middle panel of Figure 3 indicates that displacements account for a relevant part of the difference between LCM and AFC spectra, because DISP and AFC show now similar progressions, with two negative peaks in the red region of the spectrum and a sign inversion for $E-E_{0,0} \approx 0.3-0.4$ eV. Nonetheless, the spacings between the peaks are still different, as well as their relative intensities (most of all for the two negative peaks). The lower panel of Figure 3 shows that allowing the independent-mode model to consider different frequencies for the ground and excited states (DISP+FREQ) further sensibly decreases the difference with respect to AFC predictions. The residual difference, still evident in the lower panel of Figure 3, is due to the Duschinsky mixing effect; that is included in the harmonic AFC model but it is neglected in an independent-mode model as LCM.

Because Duschinsky mixings introduce band splittings, it is generally expected that they lead to a broadening of absorption spectra. However, this is not necessarily true for dichroism spectra because cancelations may happen between positive and negative intensities. In our case, cancelations yield AFC spectra narrower than those where Duschinsky coupling was neglected. The small peak in the (DISP+FREQ) spectrum arising from the 0−0 transition, and disappearing in the AFC profile, see region of $E-E_{0,0}$ around 0 eV, shows clearly that the FC/HT interference due to Duschinsky mixing may have important consequences in the case under examination.

In our previous study[20,21] on the ECD of R3MCP we have shown that first-order non-Condon vibronic effects as HT may introduce a change of sign on the chiral response of a given electronic excited state, without having to invoke the interaction with, or the superposition of peaks due to, other electronic states. This evidence may have important consequences in comparisons of theoretical and experimental ECD spectra and ultimately also in the assignment of absolute configurations. The sign reversal in the ECD response of R3MCP occurs only for the *Ax* conformer (refs 20 and 21 for details). The latter is only in a ratio of 1:9 with respect to the predominant *Eq* conformer under standard conditions, both in the gas and solvated phases. This, together with the fact that the predicted sign change appears in a narrow energy region, limits the chance that our prediction of refs 20 and 21 might be confirmed any time soon by experiment, because the feature appears to be hardly detectable, unless with a spectrometer capable of achieving very fine resolution. In the present study, the sign reversal for the TPCD signal occurs in the predominant *Eq* conformer and it survives apparently also the convolution with the chosen spectral line shape. Unfortunately, the TPCD signal for S1 is predicted to be very small, below the detection limits of the techniques available to date,[17,18] and therefore once again it is highly unlikely that our prediction might be soon confirmed by experiment. This is very regrettable because the sign reversal takes place in an energy region well separated from that where higher excited states absorb.

In Figure 4, we present the assignments of the FC, HT, and TOT stick spectra for the *Eq* conformer of R3MCP for the S1 state, obtained with the Harmonic AFC vibronic model. Convoluted spectra with a Lorentzian broadening of 0.05 eV are also included. The results for the *Ax* conformer are shown in Figure 5. Let us first discuss the *Eq* conformer. The FC contributions yield everywhere intensities of the same (negative here) sign. The lowest peak can be assigned to the 0−0 transition, whereas other intense peaks are associated to a progression along mode 30 (CO stretch). The HT peaks are both positive and negative, as we can see from the middle panel of Figure 4. However, strong cancelations between the positive and negative signals yield a convoluted HT profile showing a uniform (positive here) sign. The sign reversal survives in the TOT spectrum even after convolution. Note that the FC/HT interference plays an important role for the TOT intensity, especially in the region where the sign reversal appears. Table 2, reporting the FC, HT, and TOT intensities for some selected vibronic transitions, highlights such a role. HT yields a positive 0−0 peak, clearly of higher intensity with respect to the negative 0−0 intensity due to FC. Therefore, the weak negative signal resulting in the TOT profile must arise from the FC/HT interference. Furthermore, the strong negative intensity coming from the 0−1 transition of mode 10 (out-of-plane bending of several H atoms bound to the carbon ring) in the TOT response is likely to arise again from FC/HT interference because FC and HT yield comparable intensity (opposite sign, cf. Table 2) but both much weaker than the TOT. On the contrary, the 0−1 transition of mode 30 responsible for the strongest (negative) FC intensity in the spectrum is essentially washed out by FC/HT interference, resulting in a positive contribution to TOT. The combined band from the 0−1 transition of mode 10 and 30 ($10^1 30^1$), giving weak negative signals in both FC and HT (cf. Table 2), is also reinforced by FC/HT interference and it is responsible for a relatively strong negative signal in TOT. Strong positive FC/HT interference can also be found for the intense positive TOT signals correlated with the progression along mode 30 (30^2, 30^3, 30^4).

The *Ax* conformer shows different TPCD responses with respect to *Eq* for the S1 state, with uniform positive FC and negative (convoluted) HT signals. A sign reversal is also observed in its TOT profile, with a positive response in the lower-energy region changing to negative at higher energies. The TOT signals from the 0−0, 10^1, ($10^1 30^1$), 30^3, and 30^4 transitions are all strengthened by FC/HT interference to a different extent. Before concluding, it is worth noticing that the sign reversal for the S1 bands persists even after Boltzmann averaging over the two conformers (red line shown both in Figure 4 and Figure 5).

Before moving to Conclusions, let us briefly analyze the consequences of the choice, somewhat arbitrary, of both line shape and line width associated to our ab initio rotatory strengths. To this end, we focus on a reference spectrum, chosen to be the AFC TPCD spectrum yielded by the S1 state of the *Eq* conformer, and we report in Figure 6 the profiles resulting from a choice of a Gaussian or a Lorentzian line shape with line widths of 0.01 or 0.05 eV. Whereas the fine details are rather evidently different, the overall appearance is essentially unaffected, and the alternation of sign unaltered.

5. Conclusions

We have presented the first study, carried out employing density functional response theory combined with the Harmonic AFC vibronic model, for the vibronically resolved TPCD profiles of a typical chiral molecule, R3MCP, in the region where the first two excited electronic states appear. Satisfactorily converged vibronic spectra can be obtained by the effective selection scheme for the vibronic contributions developed in refs 27 and 28. Both the Franck−Condon and Herzberg−Teller contributions were analyzed in detail. The TPCD spectral shape has been compared to ECD signals taken from ref 21, and to OPA and TPA signals, and it was shown that the predicted differences are due to HT effects. The difference in the relative intensities and shapes of the ECD and TPCD signals of the different states of R3MCP provides a nice example of the complementary fingerprinting capability of TPCD spectroscopy with respect to ECD. When considering also

the recent advances in the experimental technique,[18] it is perhaps fair to state that TPCD might become a valuable tool in chemistry for chiral compounds. Our study was extended to cover the region where our calculations place the first six excited electronic states, by resorting for states S3 to S6 to a simpler and less computationally demanding linear coupling model. Detailed comparison between the two different vibronic models was made for S1 and S2. We report on evidence that a change of the TPCD chiral response can be introduced by the Herzberg−Teller vibronic effect even when only a single electronic excited-state is involved in the transition, which further strongly confirms our previous findings in ECD.[20,21] It is worth to notice that, strictly speaking, different signs between the total FC and HT intensities are not a prerequisite for sign-reversal, because this latter can be local in energy, and take place even if the FC and HT intensities integrated over the energy yield the same sign. Nonetheless, different signs in the FC and HT total intensities enhance the probability that the sign reversal might extend to an energy range large enough for the change not to be washed out by homogeneous or inhomogeneous broadening. The case of the S1 state of both *Eq* and *Ax* conformers represents a clear example (data in Table 1) of this situation.

Acknowledgment. This work is supported by Swedish Research Council (VR) and the National Natural Science Foundation of China (NSFC, no. Y2007B08). A grant of computer time from the Norwegian Supercomputing Program and computer resources provided by the network Village (http://village.ipcf.cnr.it) are also acknowledged.

References and Notes

(1) Tinoco, I., Jr. *J. Chem. Phys.* **1975**, *62*, 1006.
(2) Denk, W.; Svoboda, K. *Neuron.* **1997**, *18*, 351.
(3) Nakanishi, K.; Berova, N.; Woody, R. W. *Circular Dichroism: Principles and Applications*; VCH Publishers Inc.: New York, 1994.
(4) Barron, L. D. *Molecular Light Scattering and Optical Activity*; Cambridge University Press: Cambridge, 2004.
(5) Caldwell, D. J.; Eyring, H. *The Theory of Optical Activity*; Wiley-Interscience: New York, 1971.
(6) Jansík, B.; Rizzo, A.; Ågren, H. *Chem. Phys. Lett.* **2005**, *414*, 461.
(7) Rizzo, A.; Jansík, B.; Bondo Pedersen, T.; Ågren, H. *J. Chem. Phys.* **2006**, *125*, 064113.
(8) (a) Jansík, B.; Rizzo, A.; Ågren, H. *J. Phys. Chem. B* **2007**, *111*, 446. (b) Jansík, B.; Rizzo, A.; Ågren, H. *J. Phys. Chem. B* **2007**, *111*, 2409 (Erratum).
(9) Jansík, B.; Rizzo, A.; Ågren, H.; Champagne, B. *J. Chem. Theory Comput.* **2008**, *4*, 457.
(10) Szlucki, J.; Stręk, W. *J. Chem. Phys.* **1986**, *85*, 5547.
(11) Gunde, K. E.; Richardson, F. S. *Chem. Phys.* **1995**, *194*, 195.
(12) Hache, F.; Mesnil, H.; Schanne-Klein, M. C. *Phys. Rev. B* **1999**, *60*, 6405.
(13) Mesnil, H.; Hache, F. *Phys. Rev. Lett.* **2000**, *85*, 4257.
(14) Mesnil, H.; Schanne-Klein, M. C.; Hache, F.; Alexandre, M.; Lemercier, G.; Andraud, C. *Chem. Phys. Lett.* **2001**, *338*, 269.
(15) Mesnil, H.; Schanne-Klein, M. C.; Hache, F. *Phys. Rev. A* **2002**, *66*, 013802.
(16) Alexandre, M.; Lemercier, G.; Andraud, C.; Mesnil, H.; Schanne-Klein, M. C.; Hache, F. *Synth. Met.* **2002**, *127*, 135.
(17) Markowicz, P. P.; Samoc, M.; Cerne, J.; Prasad, P. N.; Pucci, A.; Ruggeri, G. *Optics Express* **2004**, *12*, 5209.
(18) De Boni, L.; Toro, C.; Hernández, F. E. *Opt. Lett*. **2008**, *33*, 2958.
(19) Rizzo, A.; Lin, N.; Ruud, K. *J. Chem. Phys.* **2008**, *128*, 164312.
(20) Lin, N.; Luo, Y.; Santoro, F.; Zhao, X.; Rizzo, A. *Chem. Phys. Lett.* **2008**, *464*, 144.
(21) Lin, N.; Santoro, F.; Zhao, X.; Rizzo, A.; Barone, V. *J. Phys. Chem. A* **2008**, *112*, 12401.
(22) Neugebauer, J.; Baerends, E. J.; Noojien, M.; Autschbach, J. *J. Chem. Phys.* **2005**, *122*, 234305.
(23) Nooijen, M. *Int. J. Quantum Chem.* **2006**, *106*, 2489.
(24) Dierksen, M.; Grimme, S. *J. Chem. Phys.* **2006**, *124*, 174301.
(25) Craig, D. P.; Small, G. J. *J. Chem. Phys.* **1969**, *50*, 3827.
(26) Duschinsky, F. *Acta Physicochim.* **1937**, *7*, 551 URSS.
(27) (a) Santoro, F.; Improta, R.; Lami, A.; Bloino, J.; Barone, V. *J. Chem. Phys.* **2007**, *126*, 084509. (b) *ibidem* 2007, *126*, 169903. (c) Santoro, F.; Lami, A.; Improta, R.; Barone, V. *J. Chem. Phys.* **2007**, *126*, 184102.
(28) Santoro, F.; Improta, R.; Lami, A.; Bloino, J.; Barone, V. *J. Chem. Phys.* **2008**, *128*, 224311.
(29) Hazra, A.; Chang, H. H.; Nooijen, M. *J. Chem. Phys.* **2004**, *121*, 2125.
(30) Hazra, A.; Nooijen, M. *Phys. Chem. Chem. Phys.* **2005**, *7*, 1759.
(31) Li, R.; Sullivan, R.; Al-Basheer, W.; Pagni, R. M.; Compton, R. N. *J. Chem. Phys.* **2006**, *125*, 144304.
(32) Al-Basheer, W.; Pagni, R. M.; Compton, R. N. *J. Phys. Chem. A* **2007**, *111*, 2293.
(33) Macák, P.; Luo, Y.; Norman, P.; Ågren, H. *Chem. Phys. Lett.* **2000**, *330*, 447.
(34) Lin, N.; Zhao, X.; Rizzo, A.; Luo, Y. *J. Chem. Phys.* **2007**, *126*, 244509.
(35) Macák, P.; Luo, Y.; Norman, P.; Ågren, H. *J. Chem. Phys.* **2000**, *113*, 7055.
(36) Wang, Y. H.; Halik, M.; Wang, C. K.; Marder, S. R.; Luo, Y. *J. Chem. Phys.* **2005**, *123*, 194311.
(37) Condon, E. U. *Rev. Mod. Phys.* **1937**, *55*, 2789.
(38) Craig, D. P.; Thirunamachandran, T. *Molecular Quantum Electrodynamics. An Introduction to Radiation Molecule Interaction*; Dover Publications, Inc.: Mineaol, NY, 1984.
(39) Power, E. A. *J. Chem. Phys.* **1975**, *63*, 1348.
(40) Meath, W. J.; Power, E. A. *J. Phys. B: At. Mol. Opt. Phys.* **1987**, *20*, 1945.
(41) Meath, W. J.; Power, E. A. *J. Mod. Opt.* **1989**, *36*, 977.
(42) Andrews, D. L. *Chem. Phys.* **1976**, *16*, 419.
(43) McClain, M. *Acc. Chem. Res.* **1974**, *7*, 129.
(44) Becke, A. D. *J. Chem. Phys.* **1993**, *98*, 5648.
(45) Becke, A. D. *Phys. Rev. A* **1988**, *38*, 3098.
(46) Lee, C.; Yang, W.; Parr, R. G. *Phys. Rev. B* **1988**, *37*, 785.
(47) Dunning, T. H., Jr. *J. Chem. Phys.* **1989**, *90*, 1007.
(48) Frisch, M. J.; Trucks, G. W.; Schlegel, H. B.; Scuseria, G. E.; Robb, M. A.; Cheeseman, J. R.; Montgomery, J. A., Jr.; Vreven, T.; Kudin, K. N.; Burant, J. C.; Millam, J. M.; Iyengar, S. S.; Tomasi, J.; Barone, V.; Mennucci, B.; Cossi, M.; Scalmani, G.; Rega, N.; Petersson, G. A.; Nakatsuji, H.; Hada, M.; Ehara, M.; Toyota, K.; Fukuda, R.; Hasegawa, J.; Ishida, M.; Nakajima, T.; Honda, Y.; Kitao, O.; Nakai, H.; Klene, M.; Li, X.; Knox, J. E.; Hratchian, H. P.; Cross, J. B.; Bakken, V.; Adamo, C.; Jaramillo, J.; Gomperts, R.; Stratmann, R. E.; Yazyev, O.; Austin, A. J.; Cammi, R.; Pomelli, C.; Ochterski, J. W.; Ayala, P. Y.; Morokuma, K.; Voth, G. A.; Salvador, P.; Dannenberg, J. J.; Zakrzewski, V. G.; Dapprich, S.; Daniels, A. D.; Strain, M. C.; Farkas, O.; Malick, D. K.; Rabuck, A. D.; Raghavachari, K.; Foresman, J. B.; Ortiz, J. V.; Cui, Q.; Baboul, A. G.; Clifford, S.; Cioslowski, J.; Stefanov, B. B.; Liu, G.; Liashenko, A.; Piskorz, P.; Komaromi, I.; Martin, R. L.; Fox, D. J.; Keith, T.; Al-Laham, M. A.; Peng, C. Y.; Nanayakkara, A.; Challacombe, M.; Gill, P. M. W.; Johnson, B.; Chen, W.; Wong, M. W.; Gonzalez, C.; Pople, J. A. *Gaussian 03*, Rev. D.01; Gaussian, Inc.: Wallingford, CT, 2004.
(49) *DALTON, A Molecular Electronic Structure Program*, Release 2.0; 2005; see http://www.kjemi.uio.no/software/dalton/dalton.html.
(50) Yanai, Y.; Tew, D. P.; Handy, N. C. *Chem. Phys. Lett.* **2004**, *393*, 51.
(51) Peach, M. J. G.; Helgaker, T.; Salek, P.; Keal, T. W.; Lutnaes, O. B.; Tozer, D. J.; Handy, N. C. *Phys. Chem. Chem. Phys.* **2006**, *8*, 558.
(52) Santoro, F. FCclasses, a Fortran 77 code, see http://village.ipcf.cnr.it.
(53) Frisch, M. J.; Trucks, G. W.; Schlegel, H. B.; Scuseria, G. E.; Robb, M. A.; Cheeseman, J. R.; Montgomery, J. A., Jr.; Vreven, T.; Scalmani, G.; Mennucci, B.; Barone, V.; Petersson, G. A.; Caricato, M.; Nakatsuji, H.; Hada, M.; Ehara, M.; Toyota, K.; Fukuda, R.; Hasegawa, J.; Ishida, M.; Nakajima, T.; Honda, Y.; Kitao, O.; Nakai, H.; Li, X.; Hratchian, H. P.; Peralta, J. E.; Izmaylov, A. F.; Kudin, K. N.; Heyd, J. J.; Brothers, E.; Staroverov, V.; Zheng, G.; Kobayashi, R.; Normand, J.; Sonnenberg, J. L.; Iyengar, S. S.; Tomasi, J.; Cossi, M.; Rega, N.; Burant, J. C.; Millam, J. M.; Klene, M.; Knox, J. E.; Cross, J. B.; Bakken, V.; Adamo, C.; Jaramillo, J.; Gomperts, R.; Stratmann, R. E.; Yazyev, O.; Austin, A. J.; Cammi, R.; Pomelli, C.; Ochterski, J. W.; Ayala, P. Y.; Morokuma, K.; Voth, G. A.; Salvador, P; Dannenberg, J. J.; Zakrzewski, V. G.; Dapprich, S.; Daniels, A. D.; Strain, M. C.; Farkas, O.; Malick, D. K.; Rabuck, A. D.; Raghavachari, K; Foresman, J. B.; Ortiz, J. V.; Cui, Q.; Baboul, A. G.; Clifford, S.; Cioslowski, J.; Stefanov, B. B.; Liu, G.; Liashenko, A.; Piskorz, P.; Komaromi, I.; Martin, R. L.; Fox, D. J.; Keith, T.; Al-Laham, M. A.; Peng, C. Y.; Nanayakkara, A.; Challacombe, M.; Chen, W.; Wong, M. W.; Pople, J. A. Gaussian Development Version, Revision F.02; Gaussian, Inc.: Wallingford, CT, 2006.

JP8105925